Available online at www.sciencedirect.com
SCIENCE DIRECT®
International Journal of Heat and Mass Transfer 49 (2006) 1340–1349
International Journal of HEAT and MASS TRANSFER
www.elsevier.com/locate/ijhmt

Effects of a vibrational heat surface on natural convection in a vertical channel flow

Wu-Shung Fu [a,*], Chien-Ping Huang [b]

[a] Department of Mechanical Engineering, National Chiao Tung University, 1001 Ta Hsueh Road, Hsinchu 30056, Taiwan, ROC
[b] Center for Environmental, Safety and Health Technology Development, Industrial Technology Research Institute, Chutung, Hsinchu 310, Taiwan, ROC

Received 31 January 2005; received in revised form 7 October 2005
Available online 19 January 2006

Abstract

A numerical simulation is performed to study effects of a vibrational heat surface on natural convection in a vertical channel flow. This subject is a kind of moving boundary problems, and the finite element method and arbitrary Lagrangian–Eulerian kinematics description method is then utilized. The main parameters of Rayleigh number, amplitude and frequency are taken into consideration, and the mechanisms are examined in detail. The results show that for the same Rayleigh number, natural convection of a vibration heat plate with a certain combination of frequency and amplitude is possibly smaller than that of a stationary state. According to the results, the critical frequency could be derived and expressed in terms of Rayleigh number and amplitude.

Keywords: Natural convection; ALE method; Vibrational heat surface

1. Introduction

A problem of natural convection on a heat surface in a channel is important and widely considered in the design of device such as dissipated fins in a heat exchanger and arrays of electric components in a computer. However, in a practical situation the devices in the system are always under dynamic situation due to the operation of the system, which results in the device being unavoidably subject to vibration motion. To validate the mechanism of natural convection on the vibrating heat surface induced by the operation of the system in the channel then becomes an urgent need for the design of precise and effective device.

In the past, numerous relating studies investigated the effect of vibration on the natural convection. Fu and Shieh [1,2] investigated the natural convection in an enclosure affected by variable acceleration and vibration, respectively. The Nusselt numbers varied with the relating parameters were obtained and concise correlation equations to predict the resonant frequency were derived. Ishida and Kimoto [3] also studied natural convection in an enclosure subject to vertical vibration. The relationships between the frequency of vibration and Nusselt number were examined. The time scale at which the autocorrelation function became $1/e$ was an important parameter in explaining the change of the time- and surface-averaged Nusselt number. Forbes et al. [4] conducted an experimental method to study the effect of vibration on natural convection in an enclosure. The maximum enhancement of heat transfer about 50% was obtained during the experiment. Besides, several familiar studies of natural and forced convections affected by a wavy flow induced by an oscillating body were presented. Ichioka et al. [5] successfully used CFD technique to study fluid elastic vibration induced by two cylinders and cylinder row. The phenomena of vortex shedding and fluid instability were examined. Baxi and Ramachandran [6] investigated natural and forced convections of a vibrating heat sphere experimentally. The Nusselt number could be negligible as the vibrational Reynolds number was less than 200. But when it was larger than 200 the

* Corresponding author. Tel.: +886 3 5712121x55110; fax: +886 3 5720634.
E-mail address: wsfu@cc.nctu.edu.tw (W.-S. Fu).

0017-9310/$ - see front matter © 2005 Elsevier Ltd. All rights reserved.
doi:10.1016/j.ijheatmasstransfer.2005.10.028

Nomenclature

f_c	vibration frequency of heating surface (s^{-1})
F_c	dimensionless vibration frequency of heating surface
F_{cc}	dimensionless critical vibration frequency
g	acceleration of gravity (m/s^2)
Gr	Grashof number
ℓ_0	height of channel (m)
ℓ_1	height from heat surface to top (m)
ℓ_2	height of heat surface (m)
ℓ_3	height from heat surface to bottom (m)
ℓ_c	vibration amplitude of heat surface (m)
L_2	dimensionless height of heat surface
L_3	dimensionless height from heat surface to bottom
L_c	dimensionless vibration amplitude of heat surface
Nu_Y	Nusselt number
Nu	average Nusselt number
$\overline{Nu}$	time-average Nusselt number
p	pressure (N/m^2)
P	dimensionless pressure
Pr	Prandtl number
Ra	Rayleigh number
t	time (s)
T	temperature (K)
T_c	ambient temperature (K)
T_h	temperature of heat surface (K)
u, v	velocities in x and y directions (m/s)
U, V	dimensionless velocities in x and y directions
u_c	vibration velocity of heat surface (m/s)
U_c	dimensionless vibration velocity of heat surface
u_m	maximum vibration velocity of heat surface (m/s)
U_m	dimensionless maximum vibration velocity of heat surface
$\hat{u}$	mesh velocity in x direction (m/s)
$\widehat{U}$	dimensionless mesh velocity in x direction
w	width of channel
x, y	Cartesian coordinates (m)
X, Y	dimensionless Cartesian coordinates
Greek symbols	
α	thermal diffusivity (m^2/s)
β	volume coefficient of expansion (K^{-1})
θ	dimensionless temperature
λ	penalty parameter
ν	kinematic viscosity (m^2/s)
ρ	density (kg/m^3)
τ	dimensionless time
τ_p	dimensionless period time

enhancement of heat transfer was remarkable and as high as seven times of the natural convection without vibration. Nicoletti [7] reported some vibratory disturbance tests to a wall in air flow conditions and found the peaks of turbulent kinetic energy to be diminished when the disturbance moved towards the kernel or undisturbed area of the flow. Krishnan and Subba Rao [8] investigated effects of vibration on heat transfer performance of a double pipes heat exchanger by experimental methods. The overall heat transfer remained independent of the frequency of vibration up to 780–840 cpm, and thereafter there was a marginal increase. Ivanova and Kozlov [9] studied influence of vertical vibration on heat transfer in a horizontal cylindrical layer. The threshold curve of wave instability was obtained and the transition from two-vortex gravitational mode of convection to multi-vortex vibrational mode at high vibrational Grashof numbers was found. Fu and Tong [10,11] studied effects of wavy flow induced by an oscillating cylinder on force convections of a flat plate and ribs mounted on a plate. The results showed that the heat transfer is enhanced remarkably in the lock-in regime. As for the subject of the natural convection on the vibrating heat surface in a channel is seldom investigated numerically.

The aim of this study is therefore to study the natural convection on a vibrating heat surface in a channel. Due to the interaction between the fluid and heat surface, the flow and thermal fields become time-dependent and belong to one kind of moving boundary problems. For simulating the problem more realistically, it is then hardly analyzed by either the Lagrangian or the Eulerian kinematic description methods solely. An arbitrary Lagrangian–Eulerian (ALE) kinematic description method [12], which combines the characteristics of the Lagrangian and Eulerian kinematic description method, is an appropriate kinematic description method to describe this problem. In the ALE method, the computational meshes may move with the fluid (Lagrangian), be held fixed (Eulerian), or be moved in prescribed way. The detail of the kinematic theory of the ALE method is delineated in Hughes et al. [13], Donea et al. [14], and Ramaswamy [15].

Consequently, the ALE method is adopted to investigate the mechanism of natural convection on the vibrating heat surface in a channel numerically. A consistent penalty finite element method is applied to solve the governing equations. The effects of Rayleigh number, vibration frequency and amplitude of the heat surface on the flow structures and heat transfer characteristics are investigated.

2. Physical model

The physical model used in this study is shown in Fig. 1. A two-dimensional vertical channel with height and width

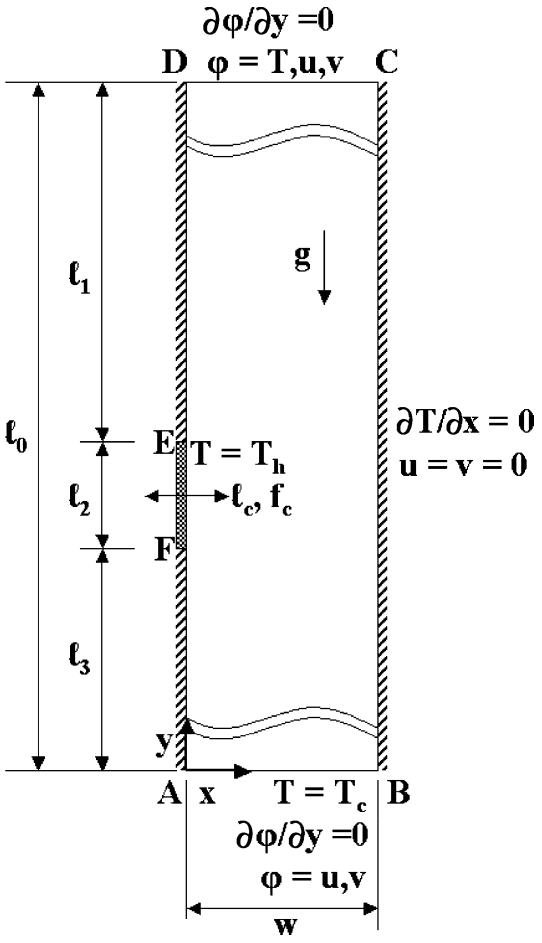

Fig. 1. Physical model.

are ℓ_0 and w, respectively. The vibrational heat surface with height ℓ_2 is on the left sidewall. The height ℓ_1 is from the top of the heat surface to the top of the channel and the height ℓ_3 is from the bottom of the heat surface to the bottom of the channel. The temperature of vibrational heat surface is constant and equal to T_h. The walls of the vertical channel are insulated except the heat surface. The ambient temperature is constant and equal to T_c. As the time $t > 0$, the heat surface is subject to vibrating motion, which is normal to the gravity direction with the frequency f_c and amplitude ℓ_c. The variations of the flow field affected by the vibrational heat surface become time-dependent and are classified into a class of moving boundary problems. As a result, the ALE method is properly utilized to analyze this subject.

The main heat transfer mechanism in this study is based on the effects of the heat fluid departed from the heat surface by the vibration motion. The direction of vibration motion of the heat surface is vertical to the channel walls, and the left wall containing the heat surface becomes convex and concave alternatively. As the heat surface is convex, the heated fluid is easily departed from the heat surface, which is beneficial to the heat transfer rate. Oppositely, the concave heat surface is disadvantageous to the heat transfer rate due to the stagnation of the heat fluid in the concavity and difficult departure from the heat surface; unless that the frequency and amplitude of vibration motion are quick and large enough to conquer the barrier (the concave situation). Then for avoiding complex calculation, the heat transfer rate of the heat device under a vibration condition is usually substituted by that under a stationary condition in most realistical situations. To validate the deviation of the heat transfer rate of the heat device under vibrational and stationary conditions and to propose useful data for thermal management in a system design become an important issue of this study.

For facilitating the analysis, the following assumptions are made.

1. The flow field is two-dimensional and laminar.
2. The fluid is air, Newtonian and incompressible.
3. The fluid properties are constant except density.
4. The non-slip condition is held on the interfaces between the fluid and heat surface.

Based upon the characteristics scales of ℓ_2, T_h and T_c, the dimensionless variables and governing equation are defined as follows:

$$X=\frac{x}{\ell_2},\quad Y=\frac{y}{\ell_2},\quad \tau=\frac{t}{t_f}=\frac{t\left(\sqrt{Ra}\cdot\alpha/\ell_2\right)}{\ell_2}$$
$$U=\frac{u}{\sqrt{Ra}\cdot\alpha/\ell_2},\quad V=\frac{v}{\sqrt{Ra}\cdot\alpha/\ell_2}$$
$$\widehat{U}=\frac{\hat{u}}{\sqrt{Ra}\cdot\alpha/\ell_2},\quad P=\frac{p}{\rho\left(\sqrt{Ra}\cdot\alpha/\ell_2\right)^2}$$
$$L_c=\frac{\ell_c}{\ell_2},\quad F_c=\frac{f_c\ell_2}{\sqrt{Ra}\cdot\alpha/\ell_2},\quad \theta=\frac{T-T_c}{T_h-T_c}$$
$$Pr=\frac{v}{\alpha},\quad Gr=\frac{g\beta(T_h-T_c)\ell_2^3}{v^2},\quad Ra=Gr\cdot Pr=\frac{g\beta(T_h-T_c)\ell_2^3}{\alpha v} \tag{1}$$

where $\hat{u}$ is the mesh velocity, ℓ_c and f_c are the vibration amplitude and frequency, respectively.

Continuity equation

$$\frac{\partial U}{\partial X}+\frac{\partial V}{\partial Y}=0 \tag{2}$$

Momentum equations

$$\frac{\partial U}{\partial\tau}+(U-\widehat{U})\frac{\partial U}{\partial X}+V\frac{\partial U}{\partial Y}=-\frac{\partial P}{\partial X}+\frac{Pr}{\sqrt{Ra}}\left(\frac{\partial^2U}{\partial X^2}+\frac{\partial^2U}{\partial Y^2}\right) \tag{3}$$
$$\frac{\partial V}{\partial\tau}+(U-\widehat{U})\frac{\partial V}{\partial X}+V\frac{\partial V}{\partial Y}=-\frac{\partial P}{\partial Y}+\frac{Pr}{\sqrt{Ra}}\left(\frac{\partial^2V}{\partial X^2}+\frac{\partial^2V}{\partial Y^2}\right)+Pr\cdot\theta \tag{4}$$

Energy equations

$$\frac{\partial\theta}{\partial\tau}+(U-\widehat{U})\frac{\partial\theta}{\partial X}+V\frac{\partial\theta}{\partial Y}=\frac{1}{\sqrt{Ra}}\left(\frac{\partial^2\theta}{\partial X^2}+\frac{\partial^2\theta}{\partial Y^2}\right) \tag{5}$$

The dimensionless vibration velocity U_c is calculated from the following equation.

$$U_c=U_m\cos(2\pi F_c\tau) \tag{6}$$

And the dimensionless maximum vibration velocity U_m can be obtained from the following equation.

$$U_m=2\pi F_c L_c \tag{7}$$

As the time $\tau>0$, the boundary conditions are as follows:

On the bottom side AB

$$\frac{\partial U}{\partial Y}=0,\quad \frac{\partial V}{\partial Y}=0,\quad \theta=0 \tag{8}$$

Except the EF surface, the other surfaces of the channel are

$$U=0,\quad V=0,\quad \frac{\partial\theta}{\partial X}=0 \tag{9}$$

On the top side CD

$$\frac{\partial U}{\partial Y}=0,\quad \frac{\partial V}{\partial Y}=0,\quad \frac{\partial\theta}{\partial Y}=0 \tag{10}$$

On the EF surface

$$U=U_c,\quad V=0,\quad \theta=1 \tag{11}$$

3. Numerical method

The governing equations and boundary conditions are solved through the Galerkin finite element formulation and a backward scheme is adopted to deal with the time terms of the governing equations. The pressure is eliminated from the governing equations using the consistent penalty method. The velocity and temperature terms are expressed as quadrilateral element and eight node quadratic Lagrangian interpolation function. The Newton–Raphson iteration algorithm is utilized to simplify the non-linear terms in the momentum equations. The discretion processes of the governing equations are similar to the one used in Fu and Yang [16].

A brief outline of the solution procedures are described as follows:

(1) Determine the optimal mesh distribution and number of the elements and nodes.
(2) Solve the values of the U, V and θ at the steady state and regard them as the initial conditions of the transient state.
(3) Determine the time step $\Delta\tau$ and the mesh velocity $\widehat{U}$ of the computational meshes.
(4) Update the coordinates of the nodes and examine the determinant of the Jacobian transformation matrix to ensure the one to one mapping to be satisfied during the Gaussian quadrature numerical integration.
(5) Solve them until the following criteria for convergence are satisfied:

$$\left|\frac{\Phi^{m+1}-\Phi^m}{\Phi^{m+1}}\right|_{\tau+\Delta\tau}<10^{-3},\quad \text{where } \Phi=U,\ V \text{ and } \theta \tag{12}$$

(6) Continue the next time step calculation until periodic solutions are attained.

4. Results and discussion

The working fluid is air with $Pr=0.71$. The main parameters of Rayleigh number Ra, vibration amplitude L_c, and vibration frequency F_c are examined.

The local Nusselt number is calculated by the following equation.

$$Nu_Y=-\left.\frac{\partial\theta}{\partial X}\right|_{X=0} \tag{13}$$

The average Nusselt number on the heat surface is expressed as follows.

$$Nu=\frac{1}{L_2}\int_{L_3}^{L_3+L_2}Nu_Y\,dY \tag{14}$$

The time-averaged Nusselt number per cycle is defined by

$$\overline{Nu}=-\frac{1}{\tau_p}\int_0^{\tau_p}Nu\,d\tau \tag{15}$$

In which τ_p is a periodical time and equals $1/F_c$.

For matching the boundary conditions at the top and bottom of the vertical channel mentioned above, the lengths from the top and bottom to the heat surface are determined by numerical tests and are equal to 80.5 and 20.5, respectively. To obtain an optimal computational mesh, four different non-uniform distributed elements are used for the mesh tests. Fig. 2 shows the velocity and temperature profiles along the line through the center of the heat surface and parallel the X-axis at the steady state under $Ra=10^3$. Based upon the results, the computational mesh with 3840 elements, which are corresponding to 12 185 nodes, are used for all cases in this study.

In addition, an implicit scheme is employed to deal with the time differential terms of the governing equations. Four different time steps $\Delta\tau=2.0\times10^{-4}$, 1.0×10^{-4}, 0.5×10^{-4}, and 0.25×10^{-4} at $Ra=10^4$, $L_c=0.1$, and $F_c=500$, are executed. The variations of the average Nusselt number on the heat surface Nu with time are shown in Fig. 3, and the time step $\Delta\tau=0.5\times10^{-4}$ is chosen for this case. But the selected time step is different for each case of different Ra and L_c in this study.

The dimensionless stream function Ψ is defined as

$$U=\frac{\partial\Psi}{\partial Y},\quad V=\frac{\partial\Psi}{\partial X} \tag{16}$$

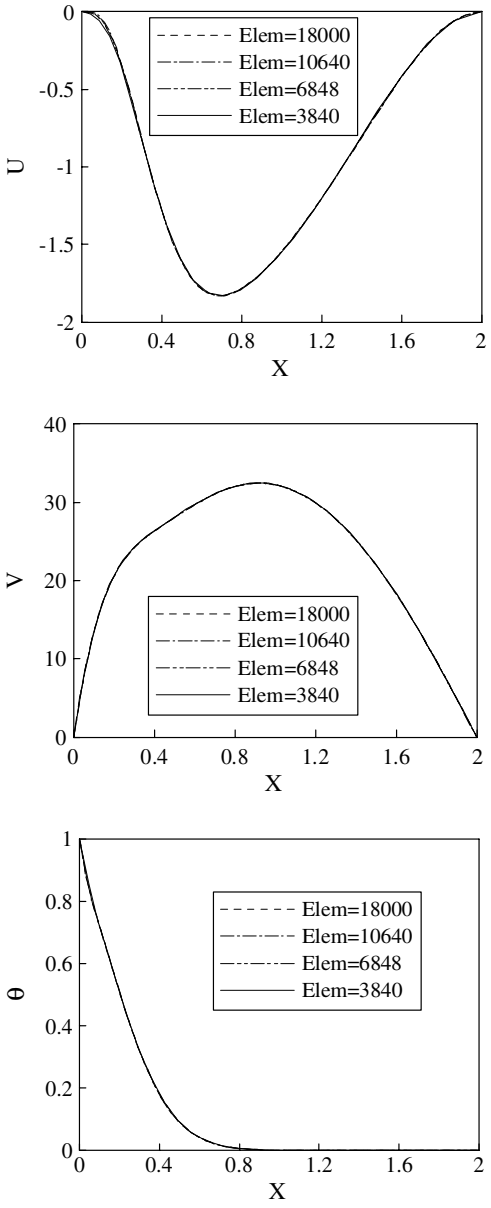

Fig. 2. Comparison of the velocity and temperature profiles along the line through the center of the heat surface and parallel the X-axis for different mesh ($Ra = 10^3$).

For clearly indicating the variations of the flow and thermal fields, the streamlines and isothermal lines in the vicinity of the heat surface are presented only. Besides, the sign "arrow" in the subsequent figures is to indicate the moving direction of the heat surface.

At practical situations, the temperature difference between the IC under the operating situation simulated by the heat surface in this study and ambient air is usually smaller than 100 °C, and the size of the IC is close to 1 cm. As a result, the range of the Rayleigh number from 10^3 to 10^5 considered in this study is adoptable.

The total region of the one wall of the channel being constant temperature was assumed in McAdams [17], and Churchill and Chu [18], and the partial region of the one

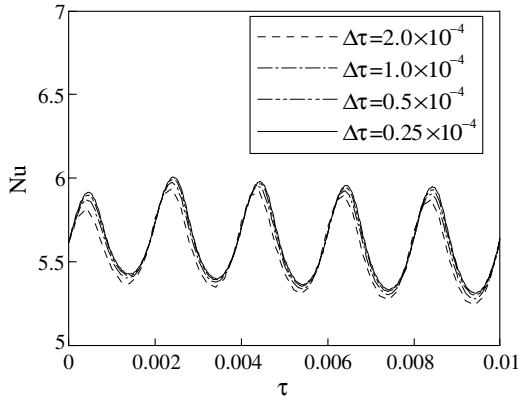

Fig. 3. Comparison of the variations of the average Nusselt numbers on the heat surface for different time step ($Ra = 10^4$, $L_c = 0.1$, $F_c = 500$).

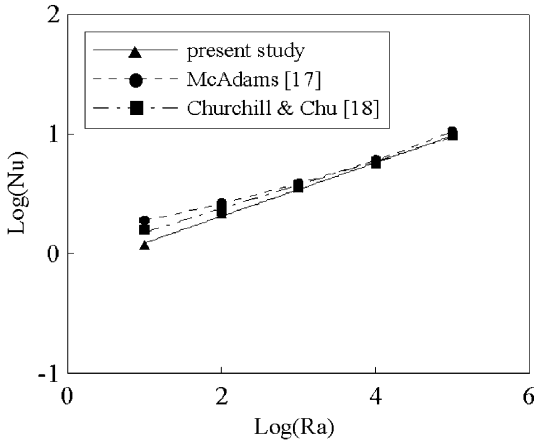

Fig. 4. Comparison with the results of the present study and those of the McAdams [17] and Churchill and Chu [18].

wall of the channel being constant temperature is simulated in the present study. Then in Fig. 4 that the average Nusselt number Nu on the heat surface affected by the entrance effect of McAdams [17] and Churchill and Chu [18] are slightly larger than those of the present study is reasonable.

The time step number of each period (period steps) is based on the results of time step test shown in Fig. 3 and is about 40. The frequency F_c is different for each case, and the dimensionless time step $\Delta\tau$ can be calculated from the following equation.

$$\Delta\tau = \frac{1}{40 \times F_c} \tag{17}$$

For better understanding of the phenomena around the vibrational heat surface, the flow and thermal fields close to the vibration surface are illustrated exclusively. Fig. 5 indicates the variations of streamlines and isothermal lines under $Ra = 10^4$, $L_c = 0.1$, and $F_c = 500$ situation during the 11th periodic cycle in which the periodical variation occurs. Fig. 5(a) is the initial stage of the 11th cycle or the final stage of the 10th cycle and $\tau = 0.02$. The position

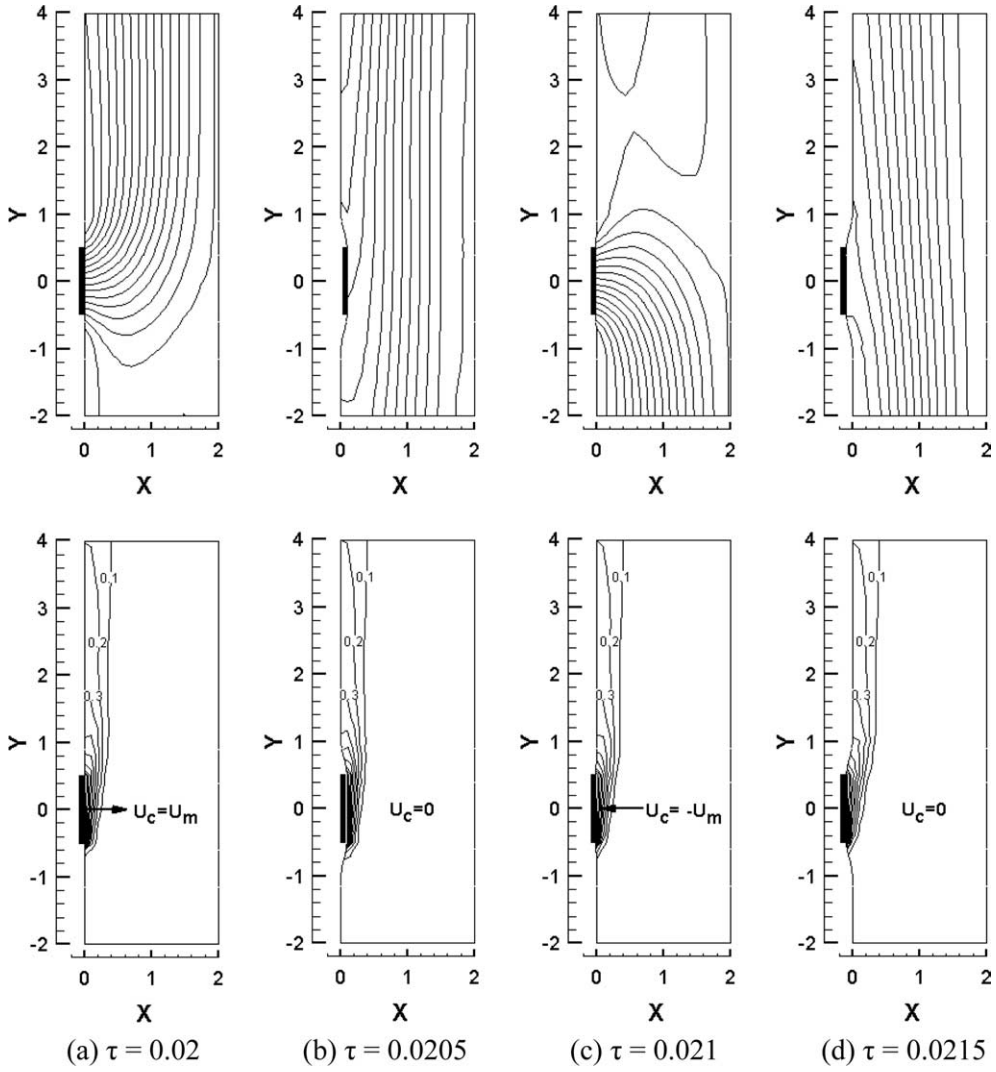

Fig. 5. The variations of the streamlines and isothermal lines during the 11th periodic cycle under $Ra = 10^4$, $L_c = 0.1$, and $F_c = 500$ situation.

of the heat surface is at the center of the vibration motion, the velocity of the heat surface moves toward the right and has the maximum speed. The fluid near the heat surface is then extruded which causes the streamlines to be ejected from the heat surface and to flow upward due to the natural convection effect. In Fig. 5(b), the heat surface is at the right most side, the motion of the heat surface stops and the velocity equals to zero. Due to the convexity of the heat surface, the phenomena of ejection of the streamlines on the heat surface and neighboring regions can be observed. In Fig. 5(c), the position of the heat surface is back to the center of the vibration motion, the velocity of the heat surface moves toward the left and has the maximum speed. Contrary to Fig. 5(b), the fluid is sucked by the heat surface, which leads the streamlines to flow toward the heat surface. In Fig. 5(d), the heat surface is at the left most side, the phenomena are similar to those shown in Fig. 5(b) but the ejection of streamlines is displaced by the suction of the streamlines. As for the isothermal lines, the variations of the distribution of isothermal lines are similar and the distributions of isothermal lines are denser near the heat surface in all the situations shown in Fig. 5.

In Fig. 6, the variations of the average Nusselt numbers Nu with time τ for $Ra = 10^3$ and $L_c = 0.1$ are indicated. Due to the vibration of the heat surface, the average Nusselt numbers vary periodically, and the more the F_c is, the larger the Nu becomes. As $F_c = 50$, most of the average Nusselt numbers are smaller than that of the stationary state (without vibration motion), and $F_c = 200$ the average Nusselt numbers are larger than that of the stationary state completely. As the heat surface is at convex situation, the variations of the average Nusselt numbers are close to the crest, oppositely, the heat surface is at concave situation, the variations of the average Nusselt numbers are close to the through.

The variations of the time-average Nusselt numbers $\overline{Nu}$ with time τ for $Ra = 10^3$ and $L_c = 0.1$ are shown in Fig. 7. When F_c is 200, the time-average Nusselt numbers are larger than that of the stationary state, and F_c is 100, the time-average Nusselt numbers decrease gradually and

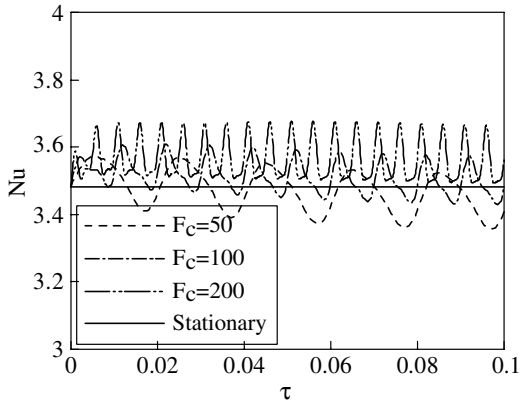

Fig. 6. The variations of the average Nusselt number Nu with time τ for $Ra = 10^3$ and $L_c = 0.1$.

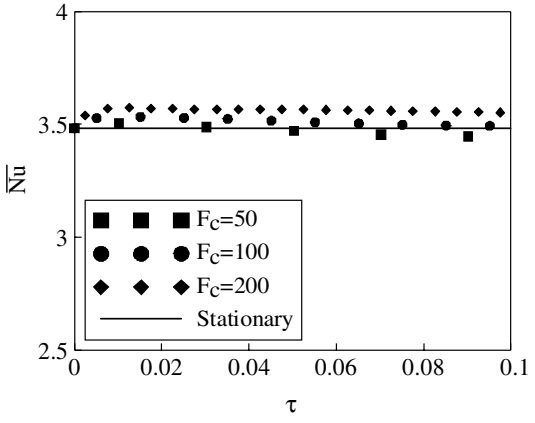

Fig. 7. The variations of the time-average Nusselt number $\overline{Nu}$ with time τ for $Ra = 10^3$ and $L_c = 0.1$.

close to that of the stationary state finally. As for $F_c = 50$, except the initial stage, the time-average Nusselt numbers are smaller than that of stationary state.

Fig. 8 indicates the variations of time-average Nusselt number $\overline{Nu}$ with time τ for $Ra = 10^4$ and $L_c = 0.1$. The Ra number increases, the time-average Nusselt numbers are simultaneously to increase for each F_c situation. Since the directions of vibration motion and natural convection motion are mutually vertical, as the heat surface is at a concave situation, which is disadvantageous to the heat transfer rate and vice versa. As a result, the interaction of both the motions mentioned above leads the magnitude of time-average Nusselt number to vary from small to large as the F_c increases.

At the same L_c (=0.1) level, as the Ra number increases to 10^5 shown in Fig. 9, the F_c must exceed 3000 which is much larger than that indicated in the cases mentioned earlier and the time-average Nusselt number $\overline{Nu}$ begins to be more than that of the stationary state. Since the higher Ra number situation means the natural convection to be drastical, the F_c of vibration motion then should be larger in order to lead the time-average Nusselt number of the vibration motion to be more than that of the stationary state.

For the same reason, shown in Fig. 10, the time-average Nusselt numbers $\overline{Nu}$ are larger than that of the stationary state only when F_c is 70 which is smaller than that

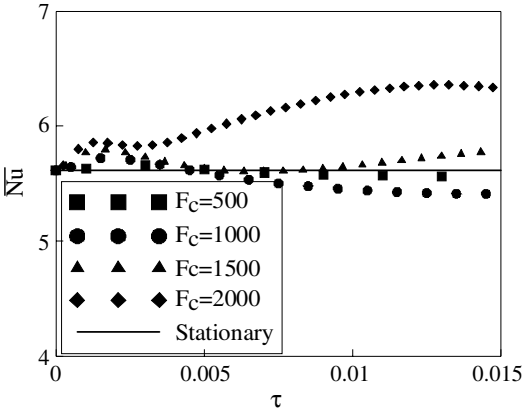

Fig. 8. The variations of the time-average Nusselt number $\overline{Nu}$ with time τ for $Ra = 10^4$ and $L_c = 0.1$.

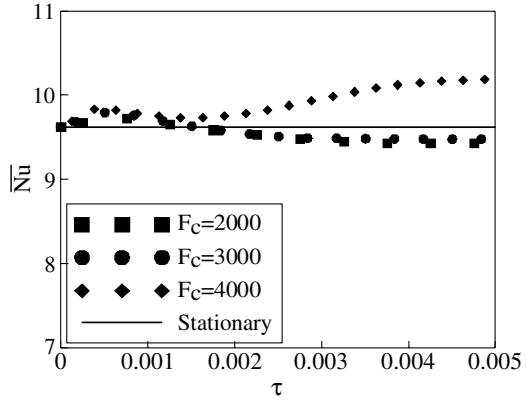

Fig. 9. The variations of the time-average Nusselt number $\overline{Nu}$ with time τ for $Ra = 10^5$ and $L_c = 0.1$.

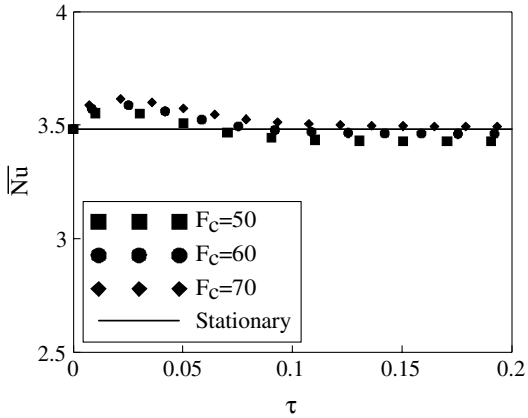

Fig. 10. The variations of the time-average Nusselt number $\overline{Nu}$ with time τ for $Ra = 10^3$ and $L_c = 0.2$.

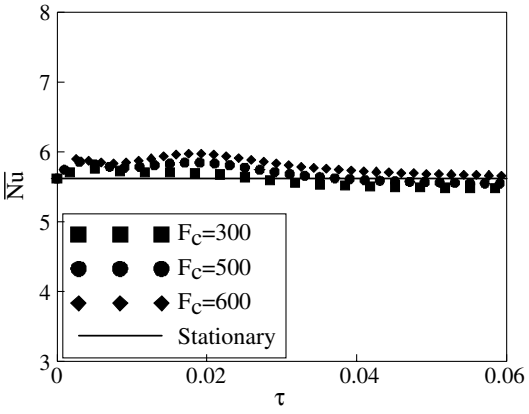

Fig. 11. The variations of the time-average Nusselt number $\overline{Nu}$ with time τ for $Ra = 10^4$ and $L_c = 0.2$.

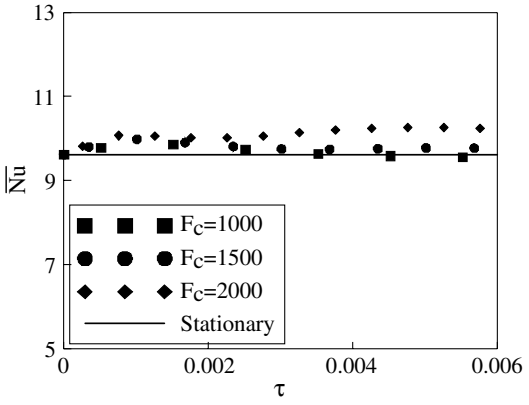

Fig. 12. The variations of the time-average Nusselt number $\overline{Nu}$ with time τ for $Ra = 10^5$ and $L_c = 0.2$.

($F_c = 100$) shown in Fig. 7 under $Ra = 10^3$ and $L_c = 0.1$ situation.

Accompanying with the increase of Ra number shown in Figs. 11 and 12, the values of F_c which cause the time-average Nusselt number to exceed those of the stationary state become larger and equal 600 and 1500, respectively, but are still smaller than those of $Ra = 10^4$, 10^5 and $L_c = 0.1$ situations shown in Figs. 8 and 9, respectively.

Due to the larger value of L_c shown in Fig. 13, then for $Ra = 10^3$ situation the F_c equals 60 at which the time-average Nusselt numbers begin to exceed that of the stationary state and is further smaller than the F_c (=100) shown in Fig. 7. Similarly, for $Ra = 10^4$ and 10^5 situations indicated in Figs. 14 and 15, respectively, when the time-average Nusselt numbers begin to be larger than those of the stationary state in the above figures, the values of the corresponding frequency F_c equal 300 and 900, respectively.

Generally, that a heat surface subject to a vibration motion is advantageous to convection heat transfer is a well-known intuition. However, based upon the results indicated above the heat transfer rates with certain combination of the F_c and L_c are possibly smaller than that of the stationary condition. Then a critical frequency F_{cc} above which the heat transfer rate of the heat surface subject to a vibration motion is larger than that of the stationary state could be defined and expressed as a function of Ra and L_c.

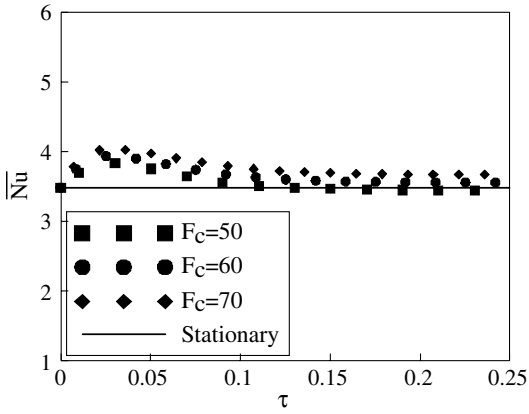

Fig. 13. The variations of the time-average Nusselt number $\overline{Nu}$ with time τ for $Ra = 10^3$ and $L_c = 0.4$.

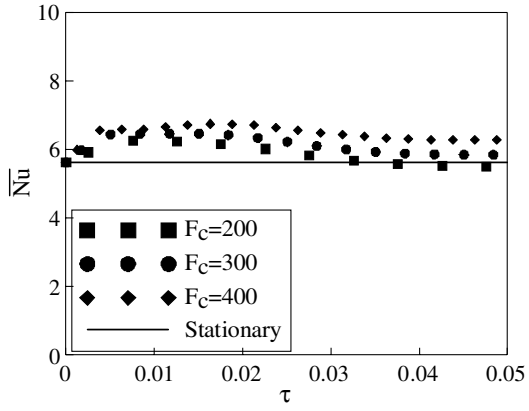

Fig. 14. The variations of the time-average Nusselt number $\overline{Nu}$ with time τ for $Ra = 10^4$ and $L_c = 0.4$.

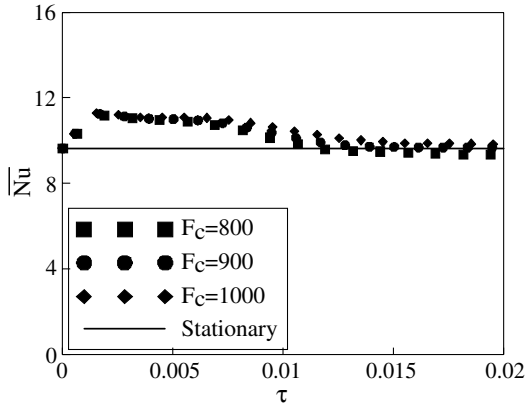

Fig. 15. The variations of the time-average Nusselt number $\overline{Nu}$ with time τ for $Ra = 10^5$ and $L_c = 0.4$.

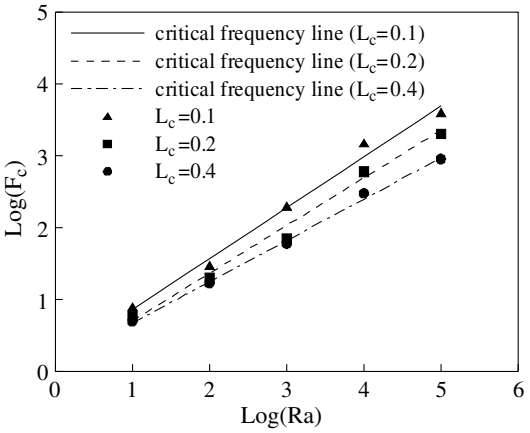

Fig. 16. The variations of the critical vibration frequency with Rayleigh number.

In Fig. 16, the heat transfer rate of each solid signal which is subject to the vibration motion for the certain L_c and F_c obtained from the results mentioned above is approximately equal to the heat transfer rate of the stationary state for the same Ra number condition. Utilize the results of the solid signals and a numerical method, the correlation equation (18) to predict the critical frequency F_{cc} could be derived.

$$\log(F_{cc}) = (-0.44L_c + 0.75)\log(Ra) + (4.9L_c^2 - 2.7L_c + 0.4) \quad (18)$$

The line, which is called a critical frequency line indicated in Fig. 16, is calculated by Eq. (18) under an assigned amplitude L_c and variation of Ra number from 10 to 10^5 conditions.

Therefore, as a region locates above the critical frequency line for an assigned amplitude L_c shown in Fig. 16, the conditions of the region which compose of the corresponding frequency F_c and Rayleigh number Ra of the region and the assigned L_c amplitude are advantageous to the heat transfer rate of the heat plate. In other words, it means the heat transfer rate of the heat plate in this region to be increased relative to that of the heat plate under the corresponding Rayleigh number mentioned above and without vibration motion.

5. Conclusions

Natural convection of a heat plate in a vertical channel under vibration motion is investigated numerically. The variations of frequency, amplitude and Rayleigh number are considered and the results are examined in detail. The main conclusions could be summarized as follows.

(1) For the same Rayleigh number, natural convection of a heat plate subject to a vibration motion under certain combination of frequency and amplitude is possibly smaller than that of a stationary state.

(2) The larger the amplitude and frequency are, the more heat transfer rate of the heat plate are obtained when the frequency is larger than the critical frequency.

(3) The critical frequency could be defined in terms of Rayleigh number and amplitude. For the same Rayleigh number and amplitude conditions, the situation of which the frequency is larger than the critical frequency is advantageous to the heat transfer and vice versa.

Acknowledgement

The support of this work by Natural Science Council, Taiwan, ROC under contact NSC 92-2212-E-009-009 is gratefully acknowledged.

References

[1] W.S. Fu, W.J. Shieh, A study of thermal convection in an enclosure induced simultaneously by gravity and vibration, Int. J. Heat Mass Transfer 35 (1992) 1695–1710.
[2] W.S. Fu, W.J. Shieh, Transient thermal convection in an enclosure induced simultaneously by gravity and vibration, Int. J. Heat Mass Transfer 36 (1993) 437–452.
[3] Hideshi Ishida, Hideo Kimoto, The structures of attractors reconstructed with time-evolution data of average heat transfer on thermal convection field in a vibrating square enclosure, Heat Transfer—Asian Res. 30 (1) (2001) 11–21.
[4] R.E. Forbes, C.T. Carley, C.J. Bell, Vibration effects on convective heat transfer in enclosure, J. Heat Transfer—Trans. ASME (1970) 429–438.
[5] T. Ichioka et al., Research on fluid elastic vibration of cylinder arrays by computational fluid dynamics (analysis of two cylinders and a cylinder row), JSME Int. J. Ser. B—Fluids Therm. Eng. 40 (1) (1997) 16–24.
[6] C.B. Baxi, A. Ramachandran, Effect of vibration on heat transfer from spheres, J. Heat Transfer—Trans. ASME (1969) 337–344.
[7] G. Nicoletti, Induced wall vibrations in air-dynamics for energy saving, Int. J. Fluid Mech. Res. 26 (5–6) (1999) 526–538.
[8] K.N. Krishnan, B.K. Subba Rao, Effect of vibration on the performance of a double pipe heat exchanger, Indian J. Technol. 13 (1975) 1–5.
[9] A.A Ivanova, V.G. Kozlov, Vibrationally gravitational convection in a horizontal cylindrical layer, Heat Transfer—Soviet Res. 20 (2) (1988) 235–247.
[10] W.S. Fu, B.H. Tong, Numerical investigation of heat transfer from a heated oscillating cylinder in a cross flow, Int. J. Heat Mass Transfer 45 (2002) 3033–3043.
[11] W.S. Fu, B.H. Tong, Numerical investigation of heat transfer characteristics of the heated blocks in the channel with a transversely oscillating cylinder, Int. J. Heat Mass Transfer 47 (2004) 341–351.
[12] C.W. Hirt, A.A. Amsden, H.K. Cooks, An arbitrary Lagrangian–Eulerian computing method for all flow speeds, J. Comput. Phys. 14 (1974) 227–253.
[13] T.J.R. Hughes, W.K. Liu, T.K. Zimmermann, Lagrangian–Eulerian finite element formulation for incompressible viscous flows, Comput. Methods Appl. Mech. Eng. 29 (1981) 329–349.
[14] J. Donea, S. Giuliani, J.P. Halleux, An arbitrary Lagrangian–Eulerian finite element method for transient dynamic fluid-structure interactions, Comput. Methods Appl. Mech. Eng. 33 (1982) 689–723.

[15] B. Ramaswamy, Numerical simulation of unsteady viscous free surface flow, J. Comput. Phys. 90 (1990) 396–430.
[16] W.S. Fu, S.J. Yang, Numerical simulation of heat transfer induced by a body moving in the same direction as flowing fluids, Heat Mass Transfer 36 (2000) 257–264.
[17] W.H. McAdams, Heat Transmission, third ed., McGraw-Hill Book Company, New York, 1954.
[18] S.W. Churchill, H.H.S. Chu, Correlating equations for laminar and turbulent free convection from a vertical plate, Int. J. Heat Mass Transfer 18 (1975) 1323–1329.